Magnetic viscosity and microstructure of GePt/FePt films

2006 J. Phys.: Condens. Matter 18 7729

(http://iopscience.iop.org/0953-8984/18/32/020)

INSTITUTE OF PHYSICS PUBLISHING JOURNAL OF PHYSICS: CONDENSED MATTER

J. Phys.: Condens. Matter **18** (2006) 7729–7736 doi:10.1088/0953-8984/18/32/020

Magnetic viscosity and microstructure of GePt/FePt films

Jai-Lin Tsai[1] **and Chia-Jen Hsu**

Department of Materials Engineering, National Chung Hsing University, 250 Kuo Kuang Road, Taichung 402, Taiwan

E-mail: tsaijl@dragon.nchu.edu.tw

Received 16 May 2006, in final form 13 July 2006
Published 31 July 2006
Online at stacks.iop.org/JPhysCM/18/7729

Abstract

We found various GePt/FePt microstructures at different post-annealing temperatures. The Ge_2Pt_3 compound was formed when the annealing temperature was 800 °C and the particle-like structure was able to relax the growth stress between Ge_2Pt_3 and quartz. After deposition of FePt film, a discontinuous $L1_0$ FePt layer was formed when it was post-annealed at 400 °C. However, isolated $L1_0$ FePt particles were observed at 800 °C post-annealing temperature, and each particle contains many grains. Furthermore, the magnetic viscosity was measured to investigate the different GePt/FePt morphology effects on thermal activation behaviour. When the applied field was less than the coercivity field H_c, we found smaller activation volume ($V_a = 0.5 \times 10^{-18}$ cm^3) for a film with 400 °C post-annealing. This is because smaller FePt grains are in between GePt islands and the moments in these grains are hard to reverse. In contrast, a larger V_a ($=1.9 \times 10^{-18}$ cm^3) was found in samples post-annealed at 600–800 °C. This is because the GePt islands agglomerate to become particle-like at high temperature and larger FePt grains were distributed on each GePt particle.

1. Introduction

The coercivity of $L1_0$ ordered FePt single crystalline or polycrystalline films (H_c) has been discussed extensively. The high coercivity originates from the large intrinsic magnetocrystalline anisotropy energy ($\sim 7 \times 10^7$ erg cm^{-3} at room temperature (RT)). For single crystalline FePt film, a highly coercivity (~60 kOe at RT) was observed in thin island-like grown film [1]. But the coercivity drops to 2 kOe when the film thickness is more than 40 nm, because there are few domain wall pinning sites in continuous single crystal film. Therefore, it is easy to obtain high coercivity in continuous FePt polycrystalline films due to the twins and anti-phase boundaries acting as domain wall pinning sites [2]. Multitwins can be

[1] Author to whom any correspondence should be addressed.

introduced from the Pt/FePt interface. These imply that the underlayer plays a significant role for FePt magnetic properties. Many researchers have chosen proper underlayers and substrates to control the FePt film orientation and reduce the ordering temperature [3–7]. Polycrystalline FePt films deposited on island-like underlayers have still not been discussed so far; we have studied the influence of island-like Ge_3Pt_2 underlayers on FePt film in previous work [8], and we study the thermal activation effect on FePt/GePt bilayer in this paper.

Magnetic viscosity measurements have been proposed as a method of understanding the magnetization reversal process in hard magnetic materials [9]. In general, we measured the coercivity as a function of temperature to study the coercivity mechanism. In most samples, the coercivities are dependent on the microstructure, and especially on the grain size. In addition, the thermal activation effect that was investigated by the magnetic viscosity effect becomes important when the grain size is very small. Linear logarithmic magnetization decay with time has been observed and the magnetic viscosity coefficient (S) is determined by the slope of magnetization (M) versus logarithm of time (t); it is a field-dependent parameter. The irreversible susceptibility (χ_{irr}) was measured from the direct current demagnetization curve (DCD). With a combination of the above two measurements, the fluctuation field (H_{f}) and the activation volume (V_{a}) have been widely estimated and discussed. In this study, we explored the thermal activation effect on different kinds of discontinuous FePt/GePt bilayer. The experimental curves (S versus H) are fitted to the simulated curves by using an analytical model proposed by Chantrell *et al* [10]. Furthermore, we have explained the switching mechanism by activation volume naturally.

2. Experimental details

RF magnetron sputter-deposited [GePt(d °C)/FePt(RT)]T °C (d being the deposition temperature; T being the post-annealing temperature) bilayers were annealed to explore the underlayer surface morphology dependence of magnetic properties. The composite FePt target was fabricated by embedding Pt square foils on a circular Fe plate, and a similar method was also used in preparing the GePt target. The film's chemical composition was obtained by inductively coupled plasma (ICP) spectroscopy. The underlayer GePt was deposited on the quartz substrate with thickness 20 nm at 800 °C and annealing for 30 min. Then FePt with fixed thickness 60 nm was grown on the underlayer that had been cooled down to room temperature. After deposition, the bilayer GePt/FePt films were post-annealed at 400–800 °C for 1 h. The base pressure of the sputtering chamber was better than 5×10^{-7} Torr and the working pressure was 10^{-2} Torr, with high purity argon gas. The crystal structure of the films was examined by grazing incident x-ray diffractometry (XRD) with Cu Kα radiation ($\lambda = 0.1541$ nm) and small slits (0.10 mm for divergent slit; 4 mm for scattering slit and receiving slit). The microstructure of the films was observed by transmission electron microscopy (TEM). Magnetic hysteresis loops were measured at room temperature by using a vibration sample magnetometer (VSM: Lakeshore 7400) with the maximum magnetic field of 1.8 T.

3. Results

3.1. Crystal structure and magnetic properties

The chemical compositions of the magnetic layer and underlayer are about $Fe_{54.9}Pt_{46.1}$ and $Ge_{40.2}Pt_{59.8}$, respectively. In our previous study, the intermetallic compound Ge_2Pt_3 phase was formed when the underlayer was deposited above 600 °C. The Ge_2Pt_3 phase formation can be explained from the reference paper [11]. In that study, the Pt layer started to react with

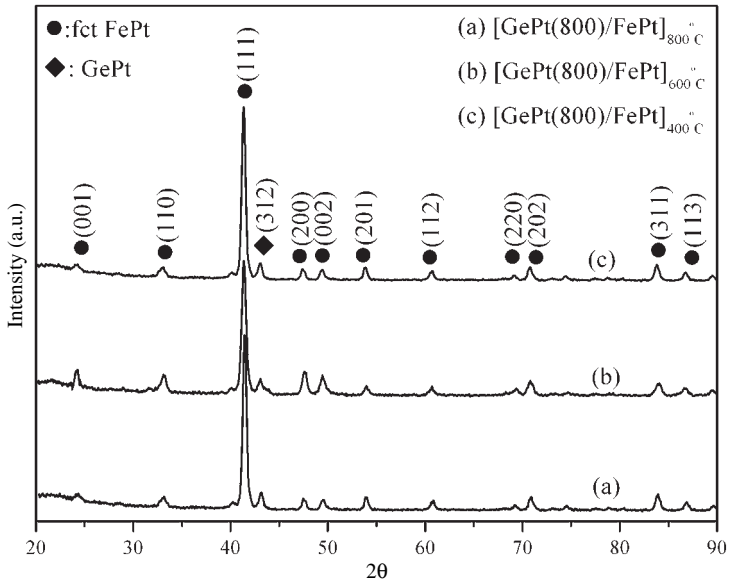

Figure 1. XRD patterns of GePt/FePt bilayers with different post-annealing temperature.

$Si_{0.75}Ge_{0.25}$ alloy films at 250 °C [11]. After annealing at 300 °C for 30 min, the entire Pt film was consumed and TEM confirmed the existence of Pt_2Si and Pt_2Ge. As a result, in the binary reaction of Pt with Ge, Pt_2Ge, PtGe, Ge_3Pt_2 and $PtGe_2$ form sequentially in the temperature range 200–400 °C. In this study, Ge_2Pt_3 phase has been formed previously, i.e., before FePt ordering in the post-annealing process.

Figure 1 shows a series of [GePt/FePt]T °C film grazing incident XRD patterns with different post-annealing temperature (T = 400, 600, 800 °C). First, we found the (001), (110) superlattice peaks that are characteristic of the ordered $L1_0$ compound phase. Second, the $L1_0$ (200), (002) peaks were split from the disordered fcc (200) peak. Also, the fcc (220) peak splits into the $L1_0$ (220) and (202) peaks. The extra $L1_0$ peaks such as (311), (201) and (112) also show the evidences of ordered isotropic FePt films.

Figure 2 shows the GePt/FePt bilayer room temperature magnetic hysteresis loops. The optimal magnetic properties were obtained when the deposition and the post-annealing temperature were equal to 800 °C for GePt and 400 °C for GePt/FePt. The island-like Ge_3Pt_2 formed completely at 800 °C with thickness 20 nm and the FePt film ordering can be enhanced on this structure. When the GePt/FePt bilayer was post-annealed at T = 800 °C, the coercivity was down to 8 kOe. This temperature is high enough to coalesce GePt/FePt in the large island structure on the quartz, and interlayer diffusion cannot be avoided. The inset in figure 2 shows initial magnetization curves of the films. It responses how fast of magnetic moments aligned in the field direction. For multi-domain particles, it describes the domain wall motion behaviour. For the film with T = 400 °C, the magnetization increased slowly up to the applied field of 8 kOe, and the domain wall pinning dominated the magnetization reversal process. For domain wall pinning type magnetization, the domain wall is pinned by defects or second precipitations at the grain boundaries and the magnetization increases slowly with the applied field. In comparison, for the film with T = 800 °C, the magnetization increased steeply, and looks like the nucleation type magnetization behaviour. For reversed domain nucleation type, the reversed domain nucleates at some grains with lower anisotropy and the magnetization

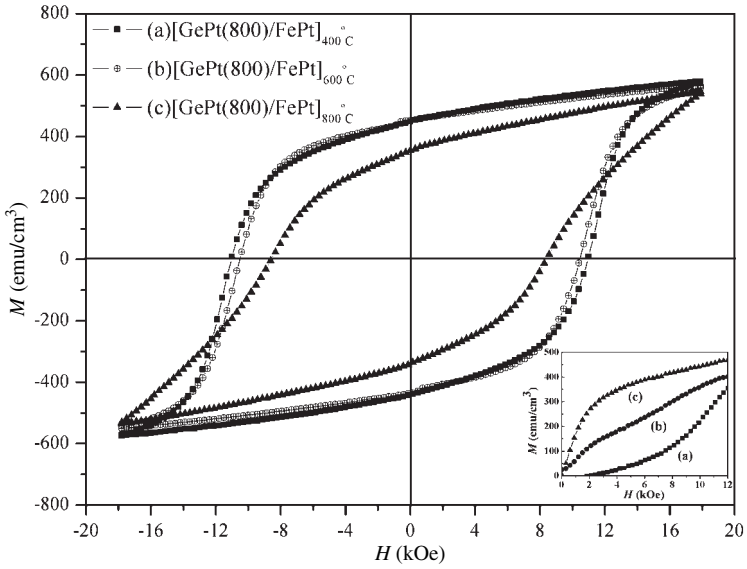

Figure 2. Room temperature hysteresis loops of GePt/FePt bilayer.

increases quickly with applied field. For the film with $T = 600\,^{\circ}\mathrm{C}$, the initial curve exhibits a mixed behaviour.

3.2. Microstructure analysis

Figure 3 shows TEM bright field images of an FePt single layer and GePt/FePt bilayer with different post-annealing temperatures. The selected area diffraction pattern (SAD) shows that all the FePt films are in the $L1_0$ ordered phase. Annealing lamellar twins are commonly observed in the long range order material as shown in figure 3(a). These twins are introduced to relieve the elastic strain distortion caused as a result of the phase transformation from face-centred-cubic (fcc) to face-centred-tetragonal (fct) structure. For the underlayer, island-like Ge_2Pt_3 nanocrystal grains were observed and the grain size ranged from 30 to 100 nm. In the as-deposited state, the Ge_2Pt_3 nanocrystal grains embedded in an amorphous quartz matrix exhibit compressive stress and post-thermal annealing for 30 min leads to stress reduction. The stress relief process is governed by the diffusive flux of quartz matrix atoms away from the local Ge_2Pt_3 grain growth region [12]. Figure 3(b) shows the bright field image of a [GePt(800 °C)/FePt (RT)]400 °C bilayer. The FePt film should be deposited on the Ge_2Pt_3 islands in area (I) or the quartz matrix in area (II) simultaneously. After post-annealing at 400 °C for 1 h, the Ge_2Pt_3 grain growth and the $L1_0$ FePt ordering was finished. More interestingly, this bilayer coercivity shown in figure 2 is much larger than that of the single layer FePt film under the same process. This can be explained by there being two areas in the FePt films. For FePt in area (I), the Ge_2Pt_3 island structure plays the role of pinning sites during domain wall motion. However, in area (II), some FePt single domain particles can be formed within 100 nm and the magnetization reversal was contributed by domain wall motion or rotation at the same time. When the FePt film was post-annealed at a higher temperature $T = 800\,^{\circ}\mathrm{C}$, all the films coalesced into a larger micron-size island and all the islands were isolated by the quartz substrate; see figure 3(c). This film shows lower coercivity (8 kOe) in figure 2, because the domain walls moved easily in each island and the demagnetization field

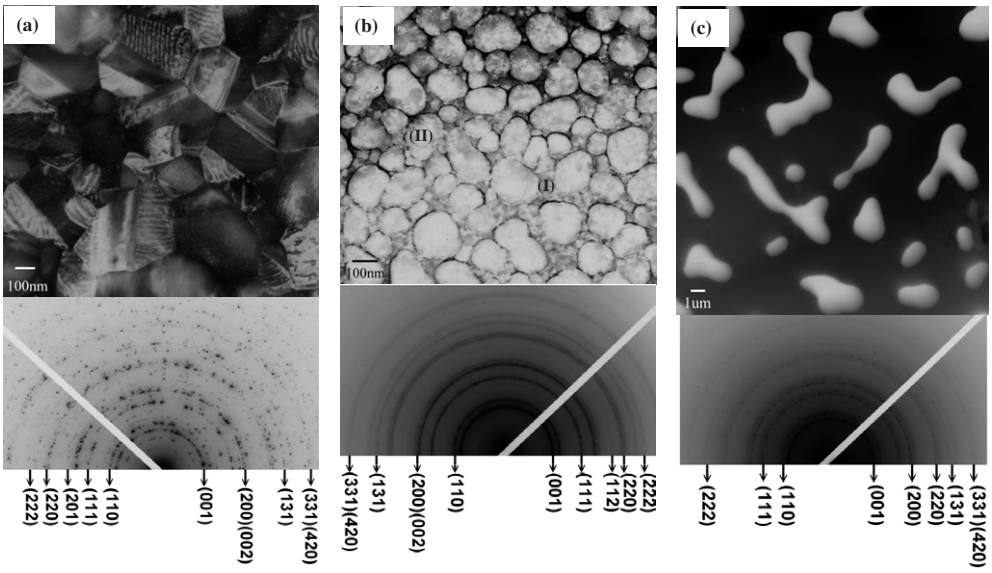

Figure 3. TEM images and SAD patterns for (a) FePt single layer, (b) [GePt(800 °C)/FePt (RT)]400 °C bilayer and (c) [GePt(800 °C)/FePt (RT)]800 °C bilayer.

due to island shape should be considered. In addition, high temperature diffusion between GePt/FePt interfaces also suppressed the FePt ordering.

3.3. Magnetic viscosity

According to the TEM observation above, the island-like Ge_2Pt_3 underlayer divided the FePt film into three kinds of microstructure with different post-annealing temperature. In figure 3, the FePt grains were distributed on the island-like Ge_2Pt_3 or quartz substrate simultaneously and the grain size distribution should be wider. Moreover, the grain size influenced the FePt film's coercivity. Therefore, the thermal activation of small grains becomes important. To investigate this effect, the magnetic viscosity measurement was performed. For the magnetic relaxation process, we first saturated the sample to the maximum applied field of 20 kOe, then different reversed field values were applied while measuring the magnetization change as a function of time for 600–1200 s. Figure 4 shows the magnetization decay as a function of logarithmic time at certain reversed field near coercivity: we found a linear relationship between magnetization (M) and log (t). Here the magnetic viscosity coefficient (S) was determined by the slope in figure 4. It was recognized by Street [13] that the exponential decay of magnetization arises from a distribution in the energy barrier, since the dependence of the energy barrier on the respective relaxation time is logarithmic. Figure 5 show the S values plotted as a function of applied field (H). The curve shows a bell shape, and the maximum S value was obtained at the coercivity (H_c) field because of the minimum energy barrier, that is, of the irreversible transition from metastable to stable states, under constant field conditions. The origin of the energy barrier is a material property, and it is related to anisotropy, shape, volume, and structure disorder. As a result, the magnetization reversal process affects the thermally activated transition.

One experimental curve was fitted to the simulated curve based on the analytical model proposed by Chantrell *et al* [10]. The essential point is the assumption of a critical energy barrier ΔE_c; kT is the thermal energy and f_0 ($\sim 10^9$ Hz) is the frequency of gyromagnetic

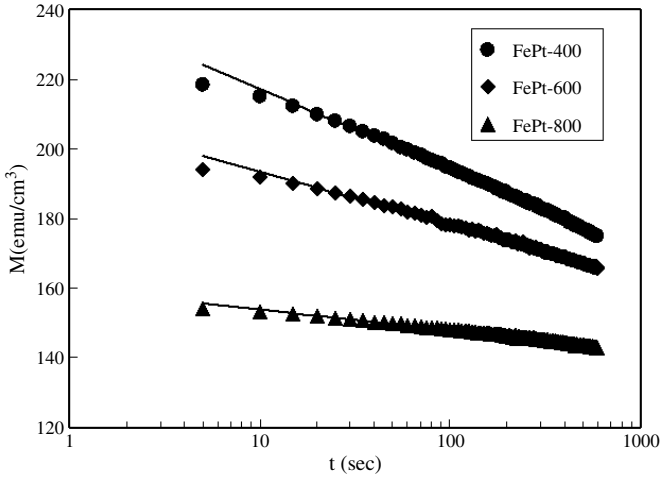

Figure 4. Magnetization as a function of time under different reversed fields: $H = -10.8$ kOe (circular), -10.3 kOe (diamond), and -8.5 kOe (triangular).

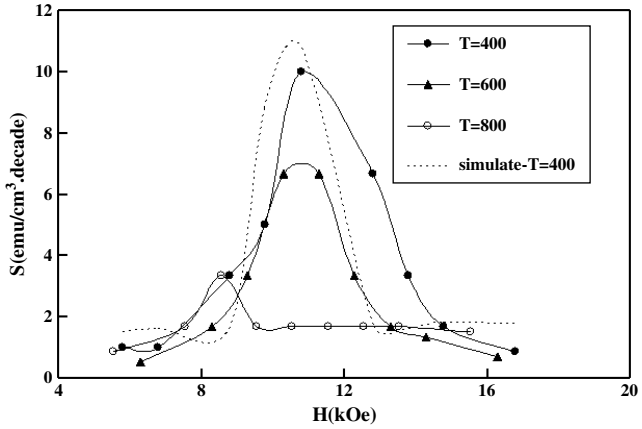

Figure 5. Magnetic viscosity coefficient as a function of applied reversed field for GePt/FePt bilayer with different post-annealing temperature.

precession. Under this assumption, when the energy barrier $\Delta E < \Delta E_c$, the sample magnetization switches to the opposite direction, otherwise, the magnetization still remains in the original direction when $\Delta E > \Delta E_c$. The calculation of the model can be simplified in the final formula of viscosity.

$$S = \frac{dM(t)}{d\ln(t)} = -\frac{AkT}{\Delta E_m} f(y_c) \qquad \text{where } A = M(t=0) - M(t=\infty)$$

$$f(y) = \frac{1}{\sqrt{2\pi} \times y \times \sigma} \exp\left[-\frac{1}{2}\left(\frac{\ln(y/y_c)}{\sigma}\right)^2\right]$$

$$\Delta E = KV_{sw}(1 - H/H_K)^2$$

$$y_c = \frac{\Delta E_c}{\Delta E_m}, \qquad y = \frac{\Delta E}{\Delta E_m}, \qquad \Delta E_c = kT \times \ln(tf_0).$$

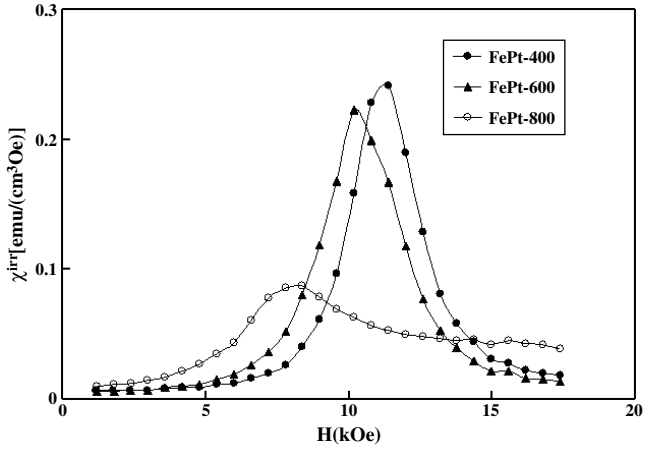

Figure 6. Irreversible susceptibility as a function of applied field for GePt/FePt bilayer.

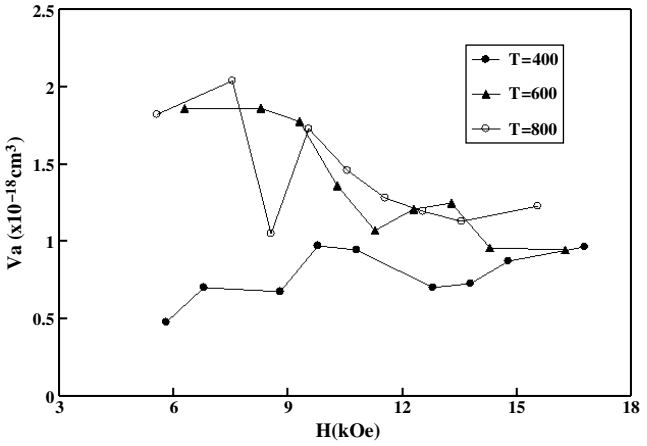

Figure 7. Activation volume as a function of applied field for GePt/FePt bilayer.

Here ΔE_{m} is the median energy barrier and $f(y)$ is the energy barrier distribution function. K and H_k are the anisotropy constant and anisotropy field. V_{sw} is the switching volume of a Stoner–Wohlfarth particle. The standard deviation $\sigma = 0.70$ is treated as the fitting parameter. In figure 5, the simulated curve almost fits to the experimental result, except for the half-width of the curve. The width of the peak may be dependent on the magnetic properties and microstructure of the film. The irreversible change of the magnetization $\mathrm{d}M_{\mathrm{irr}}$ can be induced by the change in the applied field $\mathrm{d}H$. And the irreversible susceptibility (χ_{irr}) can be derived by measuring the DC demagnetization (DCD) curve (or magnetization recoil curve). The switching field distribution curve χ_{irr}, which was obtained by differentiating the DC demagnetization curve. Figure 6 shows the plot of χ_{irr} as a function of applied field for the GePt/FePt bilayer. The curve shows a similar bell shape with the maximum value at the coercivity field. The similar shape of the $S(H)$ and χ_{irr} (H) curves suggested that thermal activation plays an important role in the magnetization reversal process. The field dependence of the activation volumes were estimated from $V_{\mathrm{a}} = (k_{\mathrm{B}} T \chi_{\mathrm{irr}})/(M_{\mathrm{s}} S)$ and are shown in figure 7. Here the ratio of S/χ_{irr} was defined as the fluctuation field H_{f}. The activation

volumes (V_a) are smaller than the average physical grain size observed in TEM. For FePt film with post-annealing temperature $T = 400\,^{\circ}\mathrm{C}$, the smaller V_a is obtained when the applied field is smaller than H_c. This suggests that some isolated small grains (figure 3(b), area I: in the gap between GePt islands) have switched independently. In contrast, for the film with $T = 600\,^{\circ}\mathrm{C}$, the larger V_a is obtained when the applied field is larger than H_c. This might be due to the exchange coupling between grains on particle-like Ge_2Pt_3, because the Ge_2Pt_3 islands aggregated to a larger particle-like structure. For the film with $T = 800\,^{\circ}\mathrm{C}$, a much smaller V_a is obtained at the coercivity field H_c. This suggests that the FePt magnetic rotation on each particle-like Ge_2Pt_3 plays an important role at the coercivity field because the FePt grains on particle-like Ge_2Pt_3 separated thoroughly, as shown in figure 3(c).

In summary, the GePt/FePt morphology was changed with different post-annealing treatment: this was proved by TEM observation. Different thermal activation behaviour was found by magnetic viscosity measurement and identified by the tendency of activation volume and magnetic viscosity coefficient (S). The relation between microstructure and physical activation volume has been suggested and discussed.

References

[1] Shima T, Takanashi K, Takahashi Y K and Hono K 2004 *Appl. Phys. Lett.* **85** 2571
[2] Takahashi Y K, Seki T O, Hono K, Shima T and Takanashi K 2004 *J. Appl. Phys.* **96** 475
[3] Tsai J L, Yuan F T and Chen S K 2005 *J. Appl. Phys.* **97** 10N122
[4] Chen J S, Lim B C and Wang J P 2003 *J. Appl. Phys.* **93** 8167
[5] Maeda T, Kai T, Kikitsu A, Nagase T and Akiyama J 2002 *Appl. Phys. Lett.* **80** 2147
[6] Ravelosona D, Chappert C, Mathet V and Bernas H 2000 *Appl. Phys. Lett.* **76** 236
[7] Lai C H, Yang C H, Chiang C C, Balaji T and Tseng T K 2004 *Appl. Phys. Lett.* **85** 4430
[8] Tsai J L, Hsu C J, Pai Y H, Shieu F S, Hsu C W, Chen S K and Chang W C 2006 *J. Magn. Magn. Mater.* **303** e258
[9] Chui S T 2000 *J. Magn. Magn. Mater.* **217** 120
[10] Chantrell R W, Lyberatos A, El-Hilo M and O' Grady K 1994 *J. Appl. Phys.* **76** 6407
[11] Hong Q Z and Mayer J W 1989 *J. Appl. Phys.* **66** 611
[12] Sharp I D *et al* 2005 *Appl. Phys. Lett.* **86** 063107
[13] Street R and Brown S D 1994 *J. Appl. Phys.* **76** 6386